I|J|A|M|B
INTERNATIONAL JOURNAL OF ADVANCES IN MEDICAL BIOTECHNOLOGY

State of the art in the use of bioceramics to elaborate 3D structures using robocasting

Juliana Kelmy Macário Barboza Daguano[1,2*]; Claudinei dos Santos[3]; Manuel Fellipe Rodrigues Pais Alves[4]; Jorge Vicente Lopes da Silva[2]; Marina Trevelin Souza[5]; Maria Helena Figueira Vaz Fernandes[6]

**Corresponding author: E-mail address:juliana.daguano@ufabc.edu.br*

Abstract: Robocasting, also known as Direct Ink Writing, is an Additive Manufacturing (AM) technique based on the direct extrusion of colloidal systems consisting of computer-controlled layer-by-layer deposition of a highly concentrated suspension (ceramic paste) through a nozzle into which this suspension is extruded. This paper presents an overview of the contributions and challenges in developing three-dimensional (3D) ceramic biomaterials by this printing method. State-of-art in different bioceramics as Alumina, Zirconia, Calcium Phosphates, Glass/Glass-ceramics, and composites is presented and discussed regarding their applications and biological behavior, in a survey comprising from the production of customized dental prosthesis to biofabricating 3D human tissues. Although robocasting represents a disruption in manufacturing porous structures, such as scaffolds for Tissue Engineering (TE), many drawbacks still remain to overcome and although widely disseminated this technique is far from allowing the obtainment of dense parts. Thus, strategies for manufacturing densified bioceramics are presented aiming at expanding the possibilities of this AM technique. The advantages and disadvantages and also future perspectives of applying robocasting in bioceramic processing are also explored.

Keywords: Additive Manufacturing (AM); Direct Ink Writing (DIW); Robocasting; Bioceramics; Challenges; Perspectives.

Introduction

Technical Approaches – Additive Manufacturing and Robocasting

By definition, Biomaterials are nonviable materials, natural or synthetic, that are useful towards the repair or even replacement of damaged body parts via interacting with living systems. The interaction of the material with the host tissue can occur at different levels, from a minimum response (inert biomaterial), to an intimate interaction with the human cells, sometimes replacing a component of the body or even carrying out their functions (bioactive or resorbable biomaterials).[1] As soon as scientists and engineers understood that it was possible to modulate the biocompatibility of materials for biomedical applications, novel and advanced manufacturing techniques were explored. Those processes aimed to produce multicomponent structures otherwise difficult to obtain using conventional routes, reduce cost and also improve performance after implantation. Within this context, Additive Manufacturing (AM) arises as a solution.

Ceramic robocasting is a direct AM technology, also named as Direct Ink Writing (DIW), based on the Material Extrusion process. In 2000, Cesarano patented and developed the technique, that consists in a computer-controlled extrusion of a viscous ceramic suspension with a high solid loading through a small orifice creating filaments that are placed in a layer-by-layer deposition process.[2] Figure 1 shows a schematic diagram illustrating this technique for obtaining of inert ceramic based on ZrO_2-Y_2O_3 (Y-TZP).

This suspension (or colloidal system) must demonstrate a suitable rheological behavior, undergoing a transformation from a pseudoplastic to a dilatant behavior when extruded in air, and following a computer-aided design model to form the 3D structures.[3] Unlike other AM techniques, as Stereolithography (SLA), Digital-Light-Processing (DLP), and Fused Deposition Material (FDM), that usually involve binder-rich contents (above 40% (v/v)) – which may lead to sudden outgassing and crack formation due to excessive shrinkage of the structure [4] – in robocasting process, concentrated ceramic suspensions are prepared using solid loading close to 40% (v/v) and dispersants/binders less than 3% (v/v).

As ceramic robocasting is not a one-step AM process, the resultant green body needs to undergo a debinding process to burn off the organic additives and a subsequent sintering process to densify the structures.[5] After drying, the materials fabricated by robocasting have a high green density (up to 60%), which allows almost complete densification upon sintering, achieving a sintered strut density near 95%.[6,7,8] A recent study explored the rapid sintering of 3D-plotted tricalcium phosphate (TCP) scaffolds with the aim of getting the on-demand scaffold fabrication closer towards the clinical practice. The rapid and reactive pressure-less sintering of β-TCP scaffolds can be achieved merely during 10 min by applying fast heating rates in the order of 100 °C/min.[9]

Robocasting appears as a new tool to process bioceramics since this is a notoriously difficult material to be processed. Firstly, due to its inherent high melting point. Ceramics usually have complex phase diagrams, which indicate that after melting new phases can form as well as unexpected

[1]Universidade Federal do ABC, Grupo de Pesquisa em Biomateriais (UFABC-GPBiomat), Alameda da Universidade, s/n, Anchieta, São Bernardo do Campo (SP), Brazil.
[2]Centro de Tecnologia da Informação – Renato Archer, Núcleo de Tecnologias Tridimensionais (CTI-NT3D), Dom Pedro I Highway (SP-65), Km 143,6 – Amarais – Techno Park, Campinas (SP), Brazil.
[3]Universidade do Estado do Rio de Janeiro, Faculdade de Tecnologia de Resende (UERJ-FAT), Rodovia Presidente Dutra, km 298, Polo Industrial, Resende (RJ), Brazil.
[4]Universidade de São Paulo, Escola de Engenharia de Lorena (USP-EEL-DEMAR), Pólo Urbo-Industrial, Gleba AI-6, s/n, Lorena (SP), Brazil.
[5]Universidade Federal de São Carlos, Laboratório de Materiais Vítreos (UFSCar-LaMaV), Rodovia Washington Luís, km 235, São Carlos (SP), Brazil.
[6]University of Aveiro, Aveiro Institute of Materials (CICECO-UA), Campus Universitário de Santiago, 3810-193 Aveiro, Portugal.

Received 09 January 2019; Accepted 20 February 2019; Available online 25 February 2019

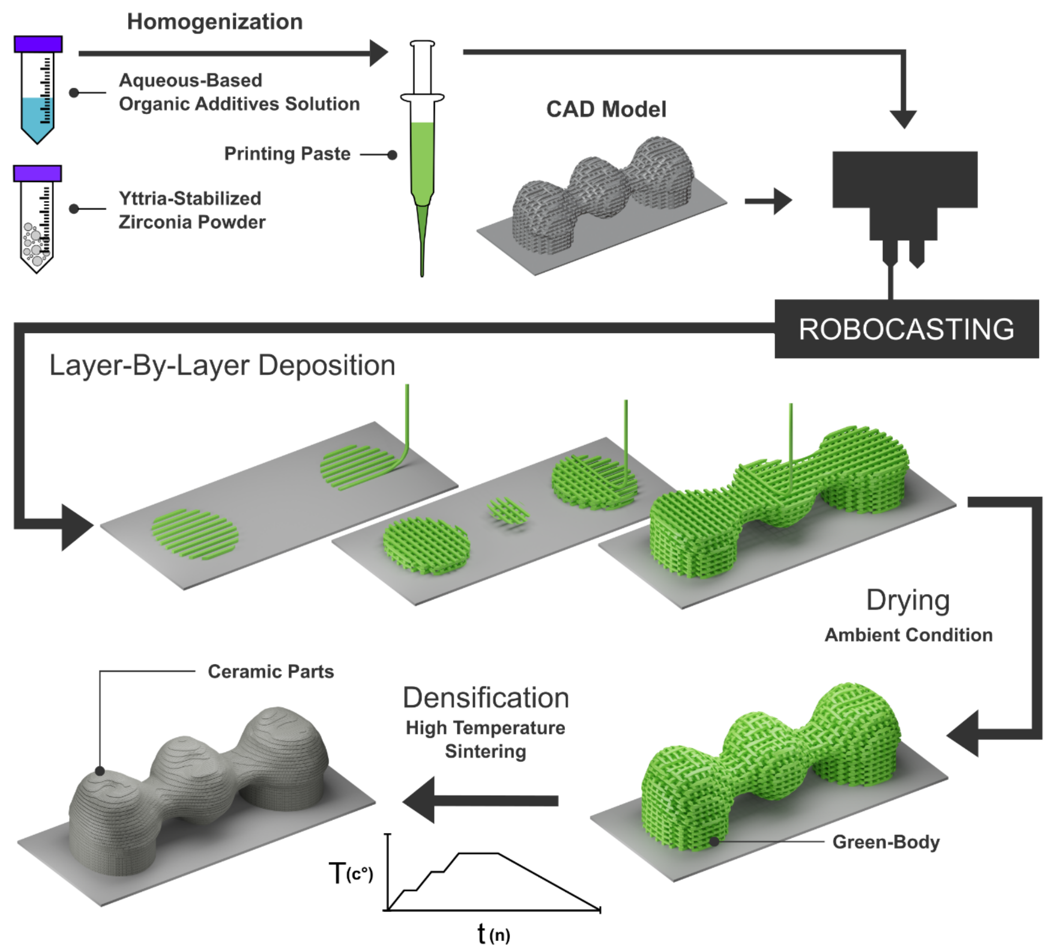

Figure 1 – Example of development steps of robocasted Y-TZP parts.

changes in their properties, even the biocompatibility. Secondly, the high-temperature processing of ceramics can cause uncontrolled porosity and cracks.[10] When it comes to porous materials for Tissue Engineering, interconnected pores are desirable to promote cellular growth and implant fixation, although they can decrease the mechanical properties of the final parts.[11,12,13] Hence, a balance between mechanical properties and biological behavior should be found for different applications.[14] An advantage of almost all ceramic systems is that ceramic powders are commercially available with a wide range of characteristics. Therefore, the possibility of using the robocasting technique, regarding the manufacture of porous or dense ceramic structures with complex morphology is particularly attractive when compared with the slurry-based methods, especially to produce biomedical devices that are aimed to meet the peculiarities of each patient.[15,16]

In this article, we aim to review the most recent contributions and challenges on porous and dense bioceramic structures obtained by the robocasting technique as well as the latest trends on 4D printing materials for biomedical applications. Some current challenges and possible solutions regarding the ideal system for the fabrication of dense robocast ceramic parts with optimal properties will be discussed with the perspective of the potential popularization and viability of this technique.

Main Challenges in Robocasting

The manufacture of dense parts by robocasting encounters severe reservations mainly because the applications of dense bioceramics are associated with the need of adequate mechanical strength and reliability for long use periods. Also, it should be considered the requirement of an appropriate biological response, independently of the particular application (dental prostheses or implants, intraoral pins, orthopedic).

Technologies that use of a large amount of volatile content such as robocasting, as ~60% of the extruded paste is composed of water and polymeric binder, debinding is a potentially problematic step when dense monolithic components are intended.

An efficient strategy to circumvent the limitation to robocasting dense parts is based on the knowledge from developing similar bioceramics, obtained by techniques that use ceramic masses such as injection molding or gelcasting.[17,18,19,20] These conventional molding methods are used for the manufacture of near-net-shape ceramics with highly complex final geometries. A major challenge is the controlling of the spatial distribution of the pores, and in the case of dense biomaterials, the control and minimization of pores and the overall porosity.

After the removal of the liquid phase or plasticizers, which is notably a very complex stage, considerably high relative densities can be achieved, depending, among other factors, mainly on the sinterability of the studied ceramic material. Currently, most ceramic suspensions or pastes used as feedstock for AM are based on significant amounts (40 to 60% v/v) of organic binders.[21,22] The efficient removal of the remaining organics requires experimental skills and acquired knowledge of the process, but many limitations still exist when it comes to monolithic structures that present a large wall thicknesses or large volumes. Thus, plasticizers should be adequately chosen because their evaporation rate is crucial for the process and it can be adapted to the specific needs of the particular AM method.

In recent years, this technique has been employed to form green parts of different ceramic structures such as alumina (Al_2O_3),[23,24] silicon carbide

(SiC),[17,25] silicon nitride (Si_3N_4),[7,26] Yttrium–stabilized zirconia (ZrO_2 / Y_2O_3),[8] and some bioactive glasses. [27,28,29] Most of the reported works include rheological studies that allow the formulation of the ideal compositions of ceramic masses and their respective optimized suspensions aiming at particular porosity and mechanical performance of the sintered parts.

Another challenge is related to mechanical properties of robocasted bioceramics. Essentially, ceramics are fragile. In this sense, a strategy proposed to ripen mechanical properties of robocast bioceramic scaffolds could be to combine the ceramic with a polymeric material. The fabrication of hybrid polymer/ceramic porous scaffolds with core/shell struts thus, appears as an interesting possibility. This strategy provides enhanced toughness without affecting, in principle, the bioactivity of the scaffold surfaces or the interconnected porosity required for bone tissue regeneration.[30] Another possibility is creating 3D Printing Bioinspired ceramic composites, using the biomimetic concept. A classic example is nacre, which boasts a combination of high stiffness, strength, and fracture toughness. Various microstructural features contribute to the toughness of nacre, including mineral bridges, nano–asperities, and waviness of the constituent platelets. In this sense, it would be possible to replicate natural structures and build highly mineralized materials that retain strength while enhancing toughness.[31]

Bioceramics for 3D printing using the Robocasting technique

Due to their unique properties, bioceramics play a privileged role within the diversity of available biomaterials.[32,33,34] The bioceramics market is expected to rise around 7% during the forecast period of 2019 – 2024.[35] This is a motivation for a fast progress in bioceramic robocasting technology, and to keep up with the growth of the market.

For a better understanding of the state–of–art of robocasting, the literature review will be divided into two sections, (i) porous bioceramics and (ii) fully dense monolithic bioceramics, as schematically distinguished in Figure 2.

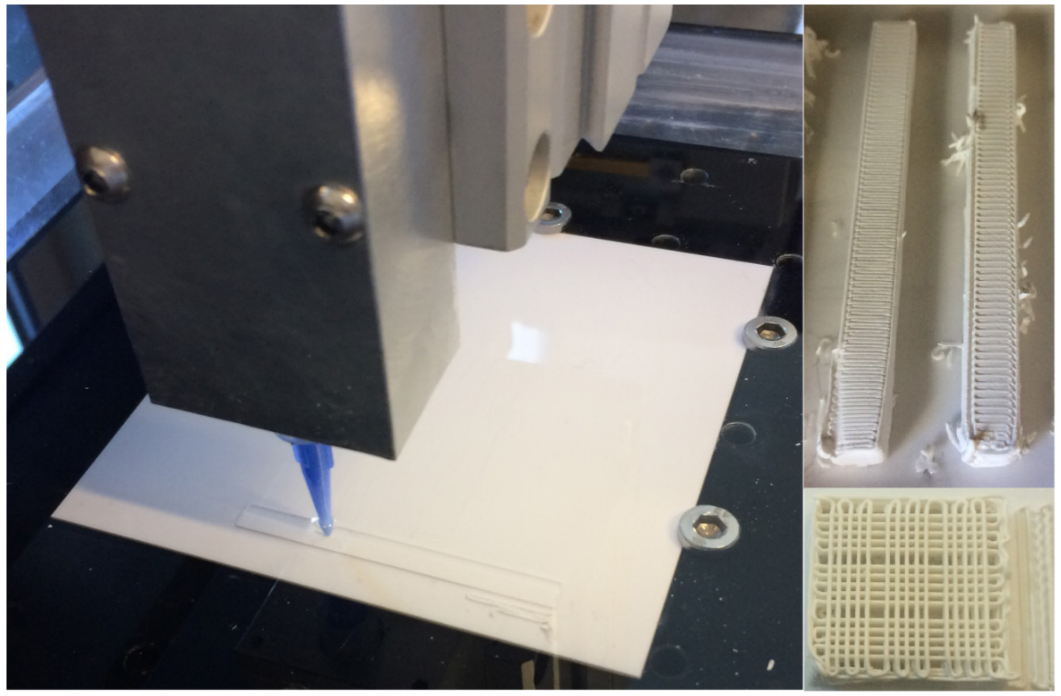

Figure 2 – Bioceramics fabricated by robocasting: (top right hand corner) fully dense monolithic parts, (bottom right hand corner) porous structures.

Porous Bioceramics

TE is a multidisciplinary research field that began in 1980's and combines engineering and life sciences in order to develop new methods for tissue replacement with improved functionality.[36] A prime step in TE is the development of complex 3D shapes with tailored external geometries, pore volume fractions, pore sizes and controlled interconnectivity. The 3D scaffolds are mainly designed to be a temporary implant, acting as a template for new cells growth while continuously and steadily degrading during/after the healing process, so that the seeded cells can grow and proliferate to regenerate into a new tissue.[37,38,39]

Currently, most of the studies have used 3D printing as a tool to make scaffolds for TE. Therefore, the microstructure features, i.e., interconnected porosity, pore size distribution, and filament aspects, are crucial factors to assure mechanical properties similar to those of the tissue and appropriate biocompatibility.[40]

Some aspects of bioceramic ink parameters, such as ink chemistry, processing additive (dispersant, binder, gelation agent), solids loading, powder reactivity, ceramic particle size, and distribution, must be understood since they have a significant effect on the printing quality. Besides, there is a strong correlation between particle size distribution and the force needed to extrude ceramic loaded inks, such that a wide particle distribution allows the formulation of higher particle loaded inks. Nommeots–Nomm et al. described how wide distributions allow for intimate packing of the particles within the ink, resulting in denser filaments post sintering. Also, they suggested that Pluronic F–127, a water soluble block co–polymer surfactant with thermally reversing rheological behaviour, consisting of poly (ethylene oxide)–poly(propylene oxide)–poly(ethylene oxide) tri–blocks (PEO–PPO–PEO), can be used as a universal binder.[41] Eqtsesadi et al. have suggested a simple recipe for robocasting 3D scaffolds. They reported that aqueous suspensions containing 45% (v/v) of 45S5 Bioglass were successfully prepared using 1 %wt carboxymethyl cellulose (CMC–250MW) as additive, tuning the rheological properties of the inks to meet the stringent requirements of robocasting. Another information is that an incomplete surface allowing bridging flocculation to occur is the key to obtain highly performing inks.[42] Recently, Koski et al. proposed a natural polymer binder system in ceramic composite scaffolds, through the utilization of naturally sourced gelatinized starch with hydroxyapatite (HA), in order to obtain green parts without the need of crosslinking or post processing.[43]

Scaffolds produced by robocasting generally possess better mechanical properties compared to those produced by indirect AM technologies, because they usually exhibit a cubic geometry with orthogonal pores, whereas scaffolds produced by other techniques mostly present a cylindrical geometry with orthogonal or radial pores. The difference in strength can reach one order of magnitude. Scaffold struts produced by robocasting can be almost dense after sintering thus improving their mechanical properties.[44,45]

Marques et al. reported the development of 3D porous calcium phosphate scaffolds by robocasting from biphasic (HA/β–TCP ≈ 1.5) powders, undoped and co–doped with Sr and Ag, where the ceramic slurry content was around 50% (v/v). After sintering at 1100 °C, scaffolds with different pore sizes and rod average diameter of 410 mm were obtained. The compressive strength was comparable to or even higher than that of cancellous bone. Sr and Ag enhanced the mechanical strength of scaffolds, conferred good antimicrobial activity against *Staphylococcus aureus* and *Escherichia coli*, and did not induce any cytotoxic effects on human MG–63 cells. Furthermore, the co–doped powder was more effective in inducing pre–osteoblastic proliferation.[46]

To meet the requirements of a 3D scaffold, *in vitro* and *in vivo* tests are key steps for the development of new suitable biomaterials. In the following tables, we present a concise review on the *in vitro* and *in vivo* assays performed with robocasted bioceramics and biocomposite scaffolds and their outcomes and relevance to the field. There is a vast literature exploring the mechanical behavior of 3D bioactive glass scaffolds manufactured by the robocasting technique, but the literature regarding the interaction of cells with bioceramic scaffolds obtained by this processing method is fairly scarce. Generally, researchers focus on constructing hybrid materials and biocomposites aiming the optimization of the process. Some interesting studies on cell viability and proliferation when in contact with robocast bioceramics and biocomposites are presented in Table 1.

Regarding in vivo tests, up to this date, the five most relevant studies using bioglasses robocast scaffolds were conducted by Liu et al. in 2013,[30,47] Deliormanli et al. in 2014,[48] Rahaman et al. in 2015,[49] and Lin et al. in 2016.[50] As to other bioceramics several studies are reported and the most important outcomes are presented in Table 2.

Authors	Material Tested	Scaffold Characteristic	Porosity	In Vitro Test	Cell Line	Time	Outcomes	Ref
Chung–Hun et al.	Sol–gel bioactive glass (70SiO_2 – 25CaO –5P_2O_5) and PCL	Degradable macro–channeled scaffolds	Pore size of 500 x 500 µm	MTT assays in static and dynamic conditions	hASCs	Up to 28 days	Cells were viable and grew actively on the scaffold assisted by the perfusion culturing (dynamic condition). Osteogenic development of hASCs was upregulated by perfusion culturing	51
Gao et al.	Gelatin + sol–gel bioactive glass (70SiO_2 – 25CaO – 5P_2O_5 mol–%)	Cubic shaped scaffolds and a grid–like microstructure	~ 30%	Cell viability and ALP activity	MC3T3–E1	Up to 21 days	Scaffolds supported cell proliferation, ALP activity, and mineralization	52
Richard et al.	β–TCP, β–TMCP, and BCMP	Inter–rod spacing of ~460 µm	β–TCP= 32% β–TCMP=45% BCMP=48%	MTT assay, ALP, Osteocalcin, TGF–β1, and Collagen	MC3T3–E1	7, 14 and 21 days	No toxicity for this cell line. Calcium nodule formation and bone markers activity suggested that the materials would induce bone formation in vivo.	53
Won et al.	Ffibronectin+ nanobioactive glass (85 SiO_2– 15CaO %wt) and PCL	Bioactive nanocomposite scaffolds	Pore size of 0.5 mm x 0.5 mm	Cell adhesion and proliferation	rMSCs	14 days	Scaffolds significantly improved cells responses, including initial anchorage and subsequent cell proliferation	54
Varanasi et al.	PCL and PLA–hydroxyapatite (70 wt–%)	2D films and 3D porous sacffolds	~76%	MTT assay	M3T3–E1	7 days	No deleterious influence of the polymer degradation products on the cells and HA acted as a support for osteoblast cytoskeletal attachment, promoting their proliferation	55
Andrade et al.	β–TCP nd gelatin	Flexible bioceramic scaffolds with pore size of ~200 µm	45%	Cell proliferation in static and dynamic conditions	MC3T3–E1	3, 7, 13 and 21 days	Both culture systems fostered cell proliferation up to day 21, however, the dynamic methodology (oscillatory flow variation) achieved a higher cell proliferation	56
Martínez–Vázquez et al.	Hydroxyapatite (HA)	Prepared by drying at room temperature or the freeze–drying method	71–77%	Cell Viability	MC3T3	1, 3, 7, and 12 days	Freeze–dried scaffolds presented a significantly increase in initial cell count and cell proliferation rate when compared to the conventional evaporation method	57
Fiocco et al.	Silica–bonded calcite	Two spacing between rods: 300 µm and 350 µm	56%–64%	Cell adhesion and distribution	ST–2 cells	1, 3, 7 and 14 days	Cells showed high metabolic activities and expressed typical osteoplastic phenotype. Mineral deposit after cell cultivation was observed and all the scaffolds stimulated cell adhesion and proliferation	58
Stanciuc et al.	Zirconia–toughened alumina (ZTA)	Robocasting of 2D pieces and 3D–ZTA scaffolds	30–50%	Cell viability, ALP activity, gene expression and minera–lization	human primary osteo–blasts (hOb)	10, 20 and 30 days	2D–ZTA presented a higher ALP activity and an increased hOb cells proliferation than the 3D–ZTA scaffolds. RUNX2 was upregulated on all samples after 10 days.	59
Ben–Arfa et al.	Sol–gel glass composition (64.4SiO_2–4.9Na_2O–21.53CaO – 9.09 P_2O_5,% wt.)	Different pore sizes = 300, 400 and 500 βm; with dimensions of 3 × 3 × 4 m	~47%	MTT assays according to ISO 10993–5 standard	MG63 osteo––blasts	7 days	Within the pore size range tested, pore size did not exert any significant influence on cell viability, presenting no cytotoxicity towards the osteoblasts	60

Table 1 – In vitro studies with robocast scaffolds from different materials.

Vol. 2 N.1, 2019 INTERNATIONAL JOURNAL OF ADVANCES IN MEDICAL BIOTECHNOLOGY – IJAMB

Authors	Material Tested	Characteristics	Porosity	In Vivo Test	Animal Model	Time	Outcomes	Ref
Liu et al.	Bioactive glass 13–93	Scaffolds BMP2 loaded and/or pretreated in phosphate solution	50%	Histomorpho-metric analysis	Calvarial defects of Ø4.6 mm in rats	6 weeks	BMP-2 pre-conditioned scaffolds significantly enhanced the capacity to support new bone formation	59
Liu et al.	Bioactive glass 13–93	6 x 6 x 6 mm scaffolds, pore width of 300 μm	47%	Mechanical properties during in vitro and in vivo tests	Subcutaneous model in rats	Up to 12 weeks	In vivo reduction in mechanical properties was greater than in vitro due to greater glass dissolution and faster conversion of the glass into HCA	30
Deliormanli et al.	Bioactive glass 13–93B	Scaffolds with different pore sizes =300, 600 and 900 μm	45–60%	Histological exploring tissue growth and blood vessel infiltration	Subcutaneous model in rats	4 weeks	All scaffolds were infiltrated with fibrous tissue and blood vessels. No difference was found in the formation of the fi-brous tissue for the different pore sizes.	60
Rahaman et al.	Bioactive glass 13–93	Scaffolds with or without BMP2 and pretreatment in phosphate solution	50%	Histological, histomorpho-metric analysis and SEM	Calvarial defects of Ø 4.6 mm in rats	6, 12 and 24 weeks	Bone regeneration increased with implantation time, and pretreating and BMP2 loading significantly enhanced the bone formation rate (for all studied times).	61
Lin et al.	Bioactive glass 13–93	Scaffolds with or without BMP2 loading	47%	Histological, SEM, and Histomor-pho-metric analysis	Calvarial defects of Ø 4.6 mm in rats	6, 12 and 24 weeks	BMP2 scaffolds significantly enhanced bone regeneration and their pores were almost completely infiltrated with la-mellar bone within 12 weeks. BMP2 scaffolds also had a sig-nificantly higher number of blood vessels at 6 and 12 weeks.	62
Simon et al.	Hydroxyapatite (HA)	Scaffolds with different rod sizes and porosities (different mac-ro-pores channels)	Different pore channels. From 250 to 750 μm^2	Micro-CT scans, histological and SEM analysis	Calvarial defects of Ø 11 mm in rabbits	8 and 16 weeks	Bone ingrowth at 8 and 16 weeks were comparable for all samples. Bone attached directly to HA rods indicating os-teoconduction.	61
Dellinger et al.	Hydroxyapatite (HA)	Scaffolds with and without BMP-2 loading	Pores of 100–700 μm	Histological analysis	Metacarpal and metatarsal bones defects of Ø 6 mm in goats	4 and 8 weeks	BMP-2 loaded scaffolds presented a significantly greater bone formation at both experimental times. The cells used the scaffolds as a template since the lamellar bone was aligned near the scaffolds' rod junctions.	62
Luo et al	$Ca_7Si_2P_2O_{16}$	Hollow-struts-packed (HSP) bioceramic scaffolds	Up to 85%	Micro-CT and histological analysis	Critical femoral bone defects of Ø8 × 10 mm in rabbits	4 and 8 weeks	HSP scaffolds possessed a superior bone-forming ability and micro-CT analysis showed that the new bone started to grow in the macropores and also into the hollow channels of the scaffolds.	63
Lin et al.	Collagen and hydro-xyapatite (CHA)	Biomimetic 3D scaffolds via a low-temperature process 3 rod widths: 300, 600 and 900 μm	72–83%	micro-CT and histological analysis	Ø 5 mm defects in the femur (condyle) of rabbits	2, 4, 8, or 12 weeks	CHA scaffolds facilitated new bone growth, as the bioma-terial was resorbed or incorporated into the newly formed bone. CHA promoted better defect repair compared to the nonprinted CHA scaffolds.	64
Shao et al.	Magnesium-doped Wollastonite/ TCP	CSi-Mg10 (10 mol% of Mg in CSi), CSi-Mg10/TCP15 (15-wt% TCP content) and pure β-TCP.	52–60%	Micro-CT, histological and me-chanical tests	Calvarial defects of Ø 8 mm in rabbits	4, 8 and 12 weeks	CSi-Mg10/TCP15 scaffolds displayed higher osteogenic capability when compared to CSi-Mg10 and β-TCP after 8 weeks. After 8 and 12, CSi-Mg10/TCP15 presented an in-crease in their mechanical properties, possibly due to the new bone tissue ingrowth into the scaffolds	65

Table 2 – In vivo studies with robocast scaffolds from different materials.

Fully dense monolithic bioceramics

When developing dense bioceramics by robocasting several parame–ters should be examined in a sequential step process that should be used to plan new studies. Based on information regarding the materials and the processing parameters, it is possible to create a robocasting suspension development strategy. This is shown in Figure 3.

Figure 3 shows the level of complexity associated with the develop–ment of new ceramic inks. It necessarily involves a technical study aimed at understanding the effects of solid fractions (particle quantities, sizes, and morphology) on the ink. At the same time, it is crucial to understand the interaction of the ceramic material with the fluid selected for the ink manufacture, i.e., which additives can be used to achieve a stable and printable suspension. Finally, it is of major importance the definition of the printing strategy and for the robocasting processing parameters to be optimized.

The following sections detail the relevant parameters to guide future developments on high densification of bioceramics.

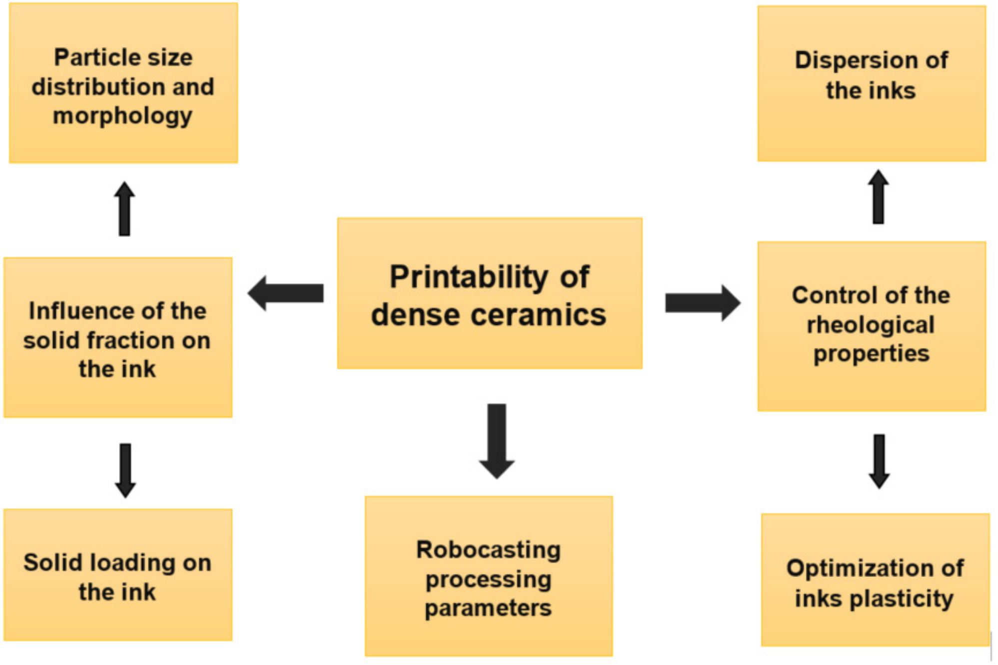

Figure 3 – Robocasting suspension development strategy.

Morphology and Particle size distribution

There is a consensus in the literature on the need for highly refined starting powders with broad particle size distribution to maximize green body compactability and sinterability.[66,67,68] In parallel, some authors state that solid loads with bimodal distributions induce a reduction of the ink's viscosity when compared to suspensions manufactured with monomodal distribution, for the same volume of suspended solids.[69,70,71]

Olhero and Ferreira fabricated three starter powder systems with va–riations in mean particle size for the preparation of trimodal suspensions. The authors found that the viscosity of the suspensions increased as the percentage of fine powders increased and, contrary to common sense, the powders with a high concentration of coarse solids showed a decrease in viscosity. This fact is due to the rheological behavior of the powders against the shear stress.[72]

Particle morphology, on the other hand, affects the rheology of sus–pensions secondarily, due to the dispersed solids content and particle size distribution, being much more impactful in colloidal suspensions. Besides, suspensions based on high aspect ratio particles, or hetero–geneous morphologies, are more susceptible to shear flow than those based on spherical particles.

Nutz et al. studied the rheology of two groups of graphite particles with different morphology, size, and surface area. The authors concluded that suspensions made with spherical particles had a significantly lower viscosity than those made with particles of anisotropic morphology.[73] Regarding the shear flow mechanism, this phenomenon is explained by the resistance promoted by the viscous suspension to the rotation of the elongated particles against the ease of spherical particles, which offer low rotational resistance.[74,75]

Figure 4 shows volumetric defects promoted by the concentric alig–nment of particles with high aspect ratio.

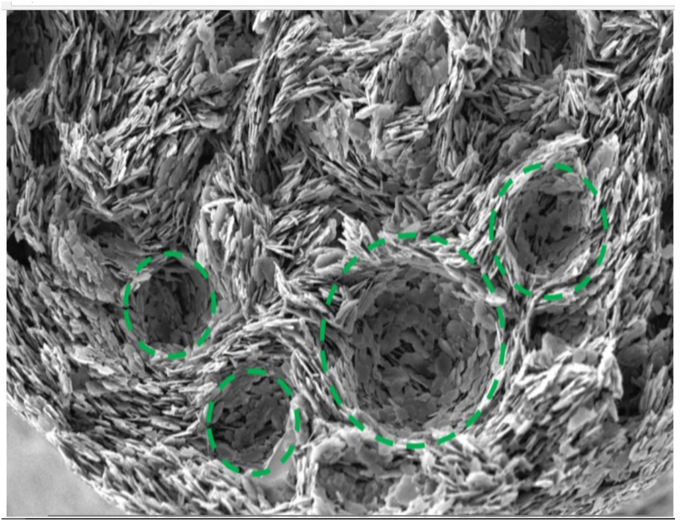

Figure 4 – Cross section of dried platelet paste, with the location of several bubbles marked. Reproduced with permission. [76]

Mass solids content

Some authors reported that, whenever possible, the ideal solids con–tent of inks for use in robocasting should be in the range of 40 to 45% and never below 30% (v/v), this would grant a dimensional and geometric predictability after sintering.[77,78] Table 3 presents some shrinkage results for different materials and additives as a function of the volume of sus–pended solids.

Materials	Additives used	Solid loading (v/v)	Linear shrinkage	Ref.
3Y-TZP	PEG-DA, DEG and Diphenyl (2,4,6- trimethylbenzoyl) phosphine oxide	37,5%	~28%	
3Y-TZP	PVA (MW 31000), PEG (MW 400), $C_6H_8O_6$ and $C_6H_8O_7$	38%	33%	8
Si_3N_4	H-PEI, L-PEI and HPMC	~35%	~28%	7
Si_3N_4	Darvan 821A, nitric acid and ammonium hydroxide	52%	16%	
Al_2O_3	Dolapix CA, magnesium chloride and Alginic acid	45%	~26%	
Al_2O_3	Darvan C-N, Bermocoll E and a polyethylene-imine solution	56%	~17%	
Al_2O_3	Dolapix CE 64, PEG 400 and methocellulose	55%	15-19%	

Table 3 – Linear shrinkage as a function of solid loading for some bioceramic inks.

Moreover, the literature reiterates that suspensions with high saturation, greater than 50% (v/v) produce parts with high densification rates and low shrinkage and warp. Nevertheless, the stabilization of suspensions with large volumes of solids requires a thorough rheological analysis, mainly due to the need of controlling the shear stresses during the extrusion process.[79,80,81] In general, the increase in mass viscosity with increasing volume of suspended solids can be directly attributed to the fact that a higher volumetric fraction of suspended ceramic particles further restricts the media flow.[82]

Rheological stabilization of suspensions

Controlling the rheological properties of the filament is essential to prevent sag and part deformation after filament extrusion, especially when geometry includes complex shapes and bridged structures such as in scaffolds. An adequate behavior can be achieved in some ways, such as by controlled flocculation of the ceramic suspension to form a gel (e.g., change in pH, solvent ionic strength, the addition of polyelectrolytes) or by using gelling additives such as a reverse thermal gel.

The literature highlights three mechanisms of solids stabilization in a suspension: electrostatic stabilization, arising from the presence of electric charges on the surface of the particles which counterbalances the attraction promoted by the van der Waals forces; steric stabilization, where the adsorption of polymers on the surface of the suspended material promotes the mechanical immobilization of the particles; and electrosteric stabilization, a combination of electrostatic and steric stabilization, where polyelectrolytes are adsorbed on the surface of the particles and ions from the dissociation of the polyelectrolytes promote an adjacent electrostatic barrier.[83,84,85] The mechanisms are demonstrated in Figure 5.

For the study of the stability of suspensions, a handy tool is the Zeta potential measurement, as it describes the potential difference between the dispersion medium and the stationary layer of boundary fluid at the surface of the dispersed particles. In other words, the technique makes it possible to assess the variation of a repulsive or attractive tendency among the solid particles as a function of the pH change in suspension and can be used to predict and control suspension stability. From this knowledge, the interaction forces can be adjusted accordingly, from a highly dispersed state in which repulsion forces dominate to a weakly flocculated or even strongly aggregated state by which attractive forces are predominant. In the case of aqueous suspensions with high solids concentration, it is common to use polyelectrolytes containing ionizable functional groups, such as amine (–NH_2) or carboxylic (–COOH), for electrostatic stabilization, in addition to pH control.[89,90,91]

Some authors support ideal rheological parameters to ensure mass printability, such as viscosity between 10 and 100 Pa.s, elastic modulus between 10^5 and 10^6 Pa and yield stress between 10^2 and 10^3 Pa. For successive printing, concentrated ceramic suspension for robocasting has to possess suitable viscoelastic properties, as described by the Herschel–Bulkley model, shear–thinning flow behavior, and possessing relatively high modulus (G') with $t_y > 200$ Pa to allow structural self–support and fabrication of high aspect ratio structures (Figure 6).[6]

For this optimization, appropriate rheological modifiers, such as floc–culating/binder agents, should be added to the already stabilized, i.e., deflocculated, suspensions.[18,79,86] In the usual approach to obtain the ideal parameters, reported in the literature, it is proposed the use of a deflocculating agent/charge binder, as opposed to the one used for the dispersion of the particles.[6,87,88] This addition intends to control flocculation by promoting a reduction of the adsorbed layer. This procedure improves a bonding effect among the particles and should be accompanied by the addition of a rheological modifier, usually a long–chain polymer, aimed at stabilizing mass plasticity (steric stabilization). Table 4 summarizes these parameters.

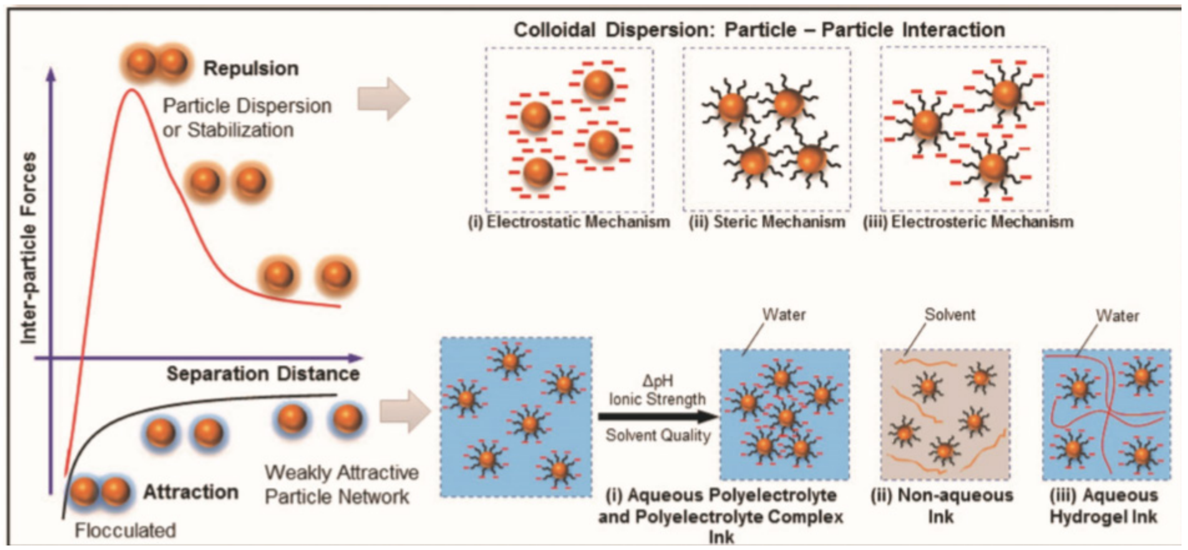

Figure 5 – Representation of mechanisms to improve the particle dispersion. Reproduced with permission. 6 Copyright 2018, John Wiley and Sons.

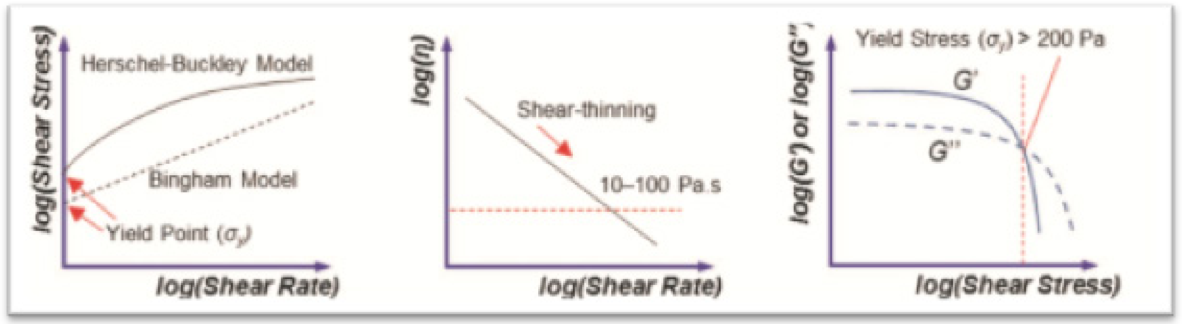

Figure 6 – Rheological behaviors required for ceramic robocasting. Reproduced with permission. [6] Copyright 2018, John Wiley and Sons.

Materials	Additives used: Dispersants	Flocculant / binder	Rheological modifier	Solid loading (v/v)	Average grain size (d_{50})	Relative density	Ref
SiC	Darvan 670, PEG 10.000 and NH_4Ac			44%	0.7 βm	~95%	89
Al_2O_3		Pluronic F–127		39%	0.3 βm	~97%	17
Al_2O_3		Darvan C, psyllium and Glycerol		49%	0.4 βm	~98%	85
Al_2O_3	Darvan 821A	PVP		55%	0.6 βm	92%	86
3Y–TZP	Dolapix CE 64/ NH_4OH			50%	0.04 βm	~99%	87
3Y–TZP	$C_6H_8O_6$ / $C_6H_8O_7$	PVA (MW 31000)	PEG (MW 400)	38%	~0.4 βm	94%	8
Si_3N_4	H–PEI/L–PEI		HPMC	52%	0.77 βm	~99%	7
Si_3N_4	H–PEI/L–PEI	Darvan–821	HPMC	44%	0.5 βm	97%	27

Table 4 – Relationship between additives used, suspended solids loading, average particle size, and relative density of the final part.

Finally, some equations are presented as support for the controlling of parameters and print design. The ideal volumetric flow rate (Q) to fill the path taken by the print nozzle, ensuring the maintenance of the predicted specimen dimensions is essential for defining the robocasting parameters. Several authors suggest Equation (1) to specify this parameter:[16,17,85,86]

$$Q = \left(\pi r^3/_4\right) \cdot \dot{\gamma} \tag{1}$$

where: Q = ideal volumetric flow rate (µm³/s), r = radius of extrusion nozzle (µm) and ($\dot{\gamma}$) = shear rate (s^{-1}).

Since suspensions used in robocasting must have a dispersed solids fraction higher than 30% (v/v), they eventually exhibit shear–thinning flow behavior. Thus, several authors claim that the Herschel–Bulkley model, Equation (2), satisfactorily describes the degree in which the ink presents a shear–thinning or shear–thickening behavior.[3,5,90]

$$\sigma = \sigma_y^{Dyn} + K\dot{\gamma}^n \tag{2}$$

where: σ = shear stress (Pa), σ_y^(D_yn) = dynamic yield stress (Pa), K = viscosity parameter (Pa.sⁿ), γ = shear rate (s^{-1}) and n = shear exponent, for $n < 1$ the fluid is shear–thinning, whereas for $n > 1$ the fluid is shear–thickening.

Smay et al. proposed another strong feature for determining printing strategy and extrusion parameters.[93] The authors described an approach to predict the maximum span by which a structure can be constructed in green without experiencing deformation, as depicted in Equation (3).[93]

$$G' \geq 1.4 \cdot \rho \cdot S^4 D \tag{3}$$

where: G' = shear modulus, ρ = specific weight of the ink, S = relation between the span length and the layer height and D = nozzle diameter.

Another challenge experienced during the printing process is the collapse of free walls, mostly associated with the rheological properties of the ink. Figure 7 exemplifies a case in which the poor stability of the ink leads to a completely collapse of the structure.

In turn, M'Barki et al. proposed an equation to define the maximum printable height (h_{max}) of a free wall, without the risk that it will of collapse due to gravitational action, Equation (4).[96]

$$h_{max} = \frac{\sigma_y^{Dyn}}{\rho g} \tag{4}$$

where: σ_y^{Dyn} is the dynamics yield stress (Pa), ρ is the specific weight of the ink and g is the gravitational contribution (9.81m/s²)

Future Perspectives

An urging trend in robocasting is 4D printing. The conception that "time" can be incorporated into the conventional concept of 3D printing as the 4th dimension is commonly known as 4D printing.[91] This novel model of printing can potentially benefit many different areas in biomedical applications, such as tissue regeneration, medical device fabrication, and drug delivery.[92]

A perceived possibility to conduct a 4D printing is to combine different materials during processing. Multi–material printing, i.e. polymer and ceramics, could prevent the secondary shaping after printing from the polymeric materials.[93] In most of the reported AM techniques, the form of the as–printed green body usually dictates the final shape of the sintered structure, while post–printing secondary shaping of the green body obtained from the AM process is minimal. However, a deep understanding on how external stimuli such as temperature, moisture, light, magnetic field, electric field, pH, ionic concentration or chemical compounds can affect the characteristics of the printed materials is yet to be established.

Another possibility in the AM field is the obtention of smart materials. Some interesting features could be achieved using this type of materials such as controlled swelling, predicted shape alterations, functionalities change and self–assembly.[94] Self–shaping geometries, like as bending, twisting or combinations of these two basic movements, can be implemented by programming the material's microstructure to undergo local anisotropic shrinkage during heat treatment, as presented in Figure 8. This functional design may be achieved by magnetically aligning functionalized ceramic platelets in a liquid ceramic suspension, subsequently consolidated through an established enzyme–catalysed reaction, and finally achieved deliberate control over shape change during the sintering step.[95]

Regarding the robocasting process, geopolymeric slurries could be

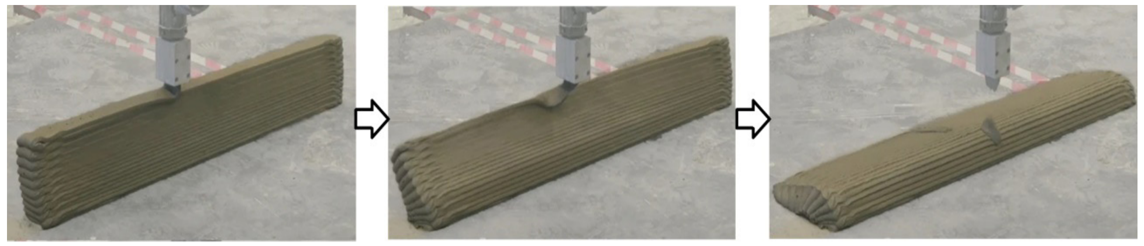

Figure 7 – Experimental buckling response of the free wall, the three stages of failure: buckling initiation, buckling development and full collapse. Reproduced with permission.[96]

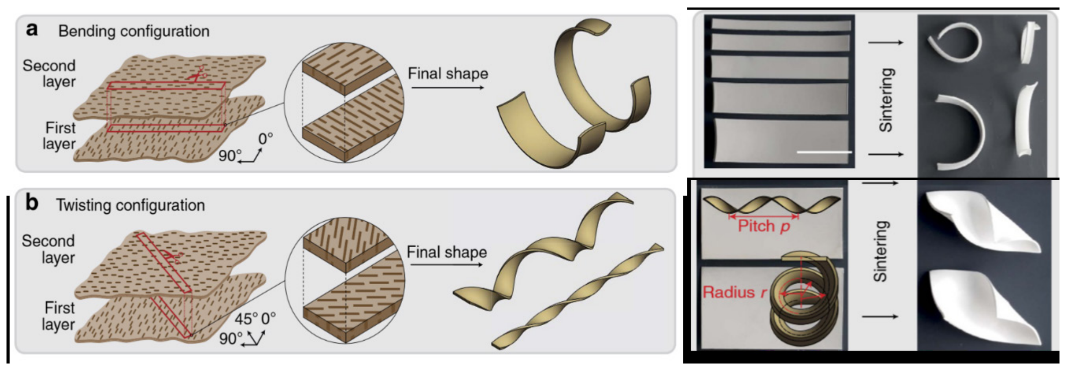

Figure 8 – Illustration of the proposed self–shaping mechanism: (a) bending and (b) twisting configuration, based on bottom–up shaping method of ceramic suspensions. Reproduced with permission.[102]

good candidates as smart materials for 4D printing provided their reaction over time could be effectively controlled.[96] However, within bioceramic content, the evidence on works reported in 4D systems does not show specific cases that support these advances.

In the last decades, a discussion on how to relate AM and TE brought up another printing concept, a new bottom–up printing system. This emerging technology, also called bioprinting, relies on the possibility of assembling building blocks (cells) that can mimic the healthy structure into larger tissue constructs. Bottom–up TE means to pattern the individual components of one tissue according to a predefined organization that guides the maturation of the construct towards a functional histo–architecture, owing in part to the promotion of cellular self–sorting and self–assembly capabilities and morphogenetic mechanisms.[97] However, for this process cells are a mandatory component of a bioink. So, obtaining a formulation that includes biologically active elements or molecules and also the biomaterials is a challenge that is still to be faced. To the best of our knowledge, up to this date, no study has been dedicated to the development of a functional bioink to be processed by robocasting. Up to now, robocasting technology has been mostly employed in the fabrication of a wide range of technical and functional scaffolds with complex morphologies. In order to push the progress of this processing method the combination of fundamental knowledge across different fields will allow the fabrication of unique and exciting architectures beyond simple robocasting technique.[5]

As presented in this review, the key factor towards multi–material printing and other AM future technologies relies on multidisciplinary research to face all the imposed challenges. Developing new ink formulations for robocasting bioprinting as well as designing smart materials will certainly expand the range of clinical applications for these materials and demonstrate the potential of AM in the biomedical field.

Acknowledgement

J Daguano and J Silva would like to thank the São Paulo Research Foundation – FAPESP, grant number 2019/11950–6. C Santos would like to thank the FAPERJ (E–26–201.476/2014) and CNPq (308684/2013–3 and 3311119/2017–4) for financial support. M Souza is grateful to the São Paulo Research Foundation – Fapesp, grant number 2013/00793–6. Also, J. Daguano is grateful to O Amorim for providing graphical art help.

MHV Fernandes acknowledges the project CICECO–Aveiro Institute of Materials, UIDB/50011/2020 & UIDP/50011/2020, financed by national funds through the Portuguese Foundation for Science and Technology/ MCTES

References

1. Salerno A, Netti PA, Introduction to biomedical foams, in Biomedical Foams for Tissue Engineering Applications, ed by Netti PA. Woodhead Publishing, pp 3–39 (2014).
2. Cesarano J, Calvert PD, and Inventor: Sandia Corporation, Assignee, Freeforming Objects with Low–Binder Slurry. US Patent 6027326 A (2000).
3. Lewis JA, Smay JE, Stuecker J, Cesarano J, Direct ink writing of threeβdimensional ceramic structures. J Am Ceram Soc 89: 3599(2006).
4. Johansson E, Lidström O, Johansson J, Lyckfeldt O, Adolfsson E, Influence of resin composition on the defect formation in alumina manufactured by stereolithography. Mater 10: 138 (2017).
5. Peng E, Zhang D, Ding J, Ceramic Robocasting: Recent Achievements, Potential, and Future Developments. Adv Mater 30 (47): 1802404(1–14) (2018).
6. Stuecker JN, Cesarano J, Hirschfeld DA, Control of the Viscous Behavior of Highly Concentrated Mullite Suspensions for Robocasting. J Mater Process Technol 142 [2] 318–25 (2003).
7. Zhao S, Xiao W, Rahaman MN, O'Brien D, Seitz–Sampson JW, Sonny Bal B, Robocasting of silicon nitride with controllable shape and architecture for biomedical applications. Int J Appl Ceram Technol 14(2): 117–127 (2017).
8. Barry III AR, Shepherd RF, Hanson JN, Nuzzo RG, Wiltzius P, Lewis JA, DirectβWrite Assembly of 3D Hydrogel Scaffolds for Guided Cell Growth. Adv Mater 21: 2407–2410 (2009).
9. Casas–Luna M, Tan H, Tkachenko S, Salamon D, Montufar EB, Enhancement of mechanical properties of 3D–plotted tricalcium phosphate scaffolds by rapid sintering. J Eur Ceram Soc 39: 4366–4374 (2019).
10. Bose S, Ke D, Sahasrabudhe H, Bandyopadhyay A, Additive manufacturing of biomaterials. Prog Mater Sci 93: 45–111 (2018).
11. Leong KF, Cheah CM, Chua CK. Solid freeform fabrication of three–dimensional scaffolds for engineering replacement tissues and organs. Biomater 24:2363–78 (2003).
12. Murphy SV, Atala A. 3D bioprinting of tissues and organs. Nat Biotechnol 32:773–85 (2014).
13. Fielding G, Bose S. SiO_2 and ZnO dopants in three–dimensionally printed tricalcium phosphate bone tissue engineering scaffolds enhance osteogenesis and angiogenesis in vivo. Acta Biomater 9:9137–48 (2013).
14. Woodfield TBF, Malda J, de Wijn J, Péters F, Riesle J, van Blitterswijk CA. Design of porous scaffolds for cartilage tissue engineering using a threedimensional fiber–deposition technique. Biomater 25:4149–61 (2004).
15. Eqtesadi S, Motealleh A, Perera FH, Miranda P, Pajares A, Wendelbo R, Guiberteau F, Ortiz AL, Fabricating geometrically–complex B_4C ceramic components by robocasting and pressureless spark plasma sintering. Scr Mater 145: 14–18 (2018).
16. Feilden E, Blanca EGT, Giuliani F, Saiz E, Vandeperre L, Robocasting of structural ceramic parts with hydrogel inks. J Eur Ceram Soc 36: 2525–2533 (2016).
17. Quackenbush CL, French K, Neil JT, Fabrication of sinterable silicon nitride by injection molding. Ceram Eng Sci Proc 3:(1–2) Chapter 3 (1982).
18. Millan AJ, Nieto MI, Moreno R, Aqueous injection moulding of silicon nitride. J Eur Ceram Soc 20:2661–2666 (2000).
19. Albano MP, Garrido LB, Processing of concentrated aqueous silicon nitride slips by slip casting. J Am Ceram Soc 81:837–844 (1998).
20. Wan T, Yao T, Hu H, Xia Y, Zuo K, Zheng Y, Fabrication of porous Si_3N_4 ceramics through a novel gelcasting method. Mater Lett 133:190–192 (2014).
21. Griffith ML, Halloran JW, Freeform Fabrication of Ceramics via Stereolithography. J Am Ceram Soc 79(10): 2601–8 (1996).
22. Homa J, Schwentenwein M, A Novel Additive Manufacturing Technology for High–Performance Ceramics, in Advanced Processing and Manufacturing Technologies for Nanostructured and Multifunctional Materials. Ceramic Engineering and Science Proceedings, ed by Ohji T, Singh M, Mathur S. John Wiley & Sons, Inc., Hoboken, NJ, pp. 33–40 (2014).
23. Cesarano J III, Segalman R, Calvert P, Robocasting provides moldless fabrication from slurry deposition. Ceram Ind 148:94–102 (1998).
24. Lewis JA, Smay JE, Stuecker J, Cesarano J III, Direct ink writing of threedimensional ceramic structures. J Am Ceram Soc 89:3599–3609 (2006).
25. Cai K, Román–Manso B, Smay JE, et al, Geometrically complex silicon carbide structures fabricated by robocasting. J Am Ceram Soc 95:2660–2666 (2012).
26. He GP, Hirschfeld DA, Cesarano JIII, Stuecker JN, Robocasting and mechanical testing of aqueous silicon nitride slurries, Technical Report, Sandia National Laboratory, SAND2000–1493C (2000).
27. Fu Q, Saiz E, Tomsia AP, Direct ink writing of highly porous and strong glass scaffolds for load–bearing bone defects repair and regeneration. Acta Biomater 7:3547–3554 (2011).
28. Liu X, Rahaman MN, Hilmas GE, Bal BS, Mechanical properties of bioactive glass (13–93) scaffolds fabricated by robotic deposition for structural bone repair. Acta Biomater 9(6):7025–7034 (2013).
29. Xiao W, Zaeem MA, Bal BS, Rahaman MN, Creation of bioactive glass (13–93) scaffolds for structural bone repair using a combined finite element modeling and rapid prototyping approach. Mater Sci Eng C 68:651–662 (2016).
30. Paredes C, Martínez–Vázquez FJ, Pajares A, Miranda P, Novel strategy for toughening robocast bioceramic scaffolds using polymeric cores. Ceram Int 45:19572–19576 (2019).
31. Gu GX, Libonati F, Wettermark SD, Buehler MJ, Printing nature: Unraveling the role of nacre's mineral bridges. J Mech Behav Biomed Mater 76: 135–144 (2017).
32. Soon G, Pingguan–Murphy B, Lai KW, Akbar SA, Review of zirconia–based bioceramic: Surface modification and cellular response. Ceram Int 42(11): 12543–12555 (2016).
33. Baino F, Novajra G, Vitale–Brovarone C. Bioceramics and Scaffolds: A Winning Combination for Tissue Engineering. Front Bioeng Biotechnol 3:202 (2015).
34. Hongshi Ma, Chun Feng, Jiang Chang, Chengtie Wu, 3D–printed bioceramic scaffolds: From bone tissue engineering to tumor therapy. Acta Biomater 79: 37–59 (2018).
35. Mordor Intelligence, Bioceramics Market – Growth, Trends, And Forecast (2019 – 2024). https://www.mordorintelligence.com/industry–reports/bioceramics–market [accessed 9 September 2019].
36. Cengiz IF, Pitikakis M, Cesario L, Parascandolo P, Vosilla L, Viano G, et al., Building the basis for patient–specific meniscal scaffolds: from human knee MRI to fabrication of 3D printed scaffolds. Bioprint 1: 1–10 (2016). doi:10.1016/j.bprint.2016.05.001
37. Do AV, Khorsand B, Geary SM, Salem AK, 3D printing of scaffolds for tissue regeneration applications. Adv Healthc Mat 4: 1742–1762. (2015). doi: 10.1002/adhm.201500168
38. Duarte Campos DF, Blaeser A, Buellesbach K, Sen KS, Xun W, Tillmann W, et al., Bioprinting organotypic hydrogels with improved mesenchymal stem cell remodeling and mineralization properties for bone tissue engineering. Adv Healthc Mater 5: 1336–1345 (2016). doi: 10.1002/adhm.201501033
39. Jang J, Park HJ, Kim SW, Kim H, Park JY, Na SJ, et al., 3D printed complex tissue construct using stem cell–laden decellularized extracellular matrix bioinks for cardiac repair. Biomater 112: 264–274 (2017). doi:10.1016/J.BIOMATERIALS.2016.10.026
40. Hwa LC, Rajoo S, Noor AM, Ahmad N, Uday MB, Recent advances in 3D printing of porous ceramics: A review. Curr Opinion Sol State Mater Sci 21: 323–347 (2017).
41. Nommeots–Nomm A, Lee PD, Jones JR. Direct ink writing of highly bioactive glasses. J Eur Ceram Soc 38: 837–844 (2018).
42. Eqtesadi S, Motealleh A, Miranda P, Lemos A, Rebelo A, Ferreira JMF. A simple recipe for direct writing complex 45S5 Bioglass 3D scaffolds. Mater Letters 93: 68–71 (2013).
43. Koski C, Onuike B, Bandyopadhyay A, Bose S. Starch–hydroxyapatite composite bone scaffold fabrication utilizing a slurry extrusion–based solid freeform fabricator. Addit Manuf 24: 47–59 (2018).
44. Miranda P, Pajares A, Saiz E, Tomsia AP, Guiberteau F, Fracture Modes Under Uniaxial Compression in Hydroxyapatite Scaffolds Fabricated by Robocasting. J Biomed Mater Res A 83A(3): 646–55 (2007).
45. Dellinger JG, Cesarano J, Jamison RD, Robotic Deposition of Model Hydroxyapatite Scaffolds with Multiple Architectures and Multiscale Porosity for Bone Tissue Engineering. J Biomed Mater Res A, 82A(2): 383–94 (2007).
46. Marques CF, Perera FH, Marote A, Ferreira S, Vieira SI, Olhero S, Miranda P, Ferreira JMF, Biphasic calcium phosphate scaffolds fabricated by direct write assembly: Mechanical, anti–microbial and osteoblastic properties. J Eur Ceram Soc 37(1):359–368 (2017).
47. Chung–Hun OH, Seok–Jung Hong, IJ, Hye–Sun Y, Seung–Hwan J, Hae–Won K, Development of Robotic Dispensed Bioactive Scaffolds and Human Adipose–Derived Stem Cell Culturing for Bone Tissue Engineering. Tissue Eng Part C 16(4): 561–71 (2010). doi: 10.1089=ten.tec.2009.0274
48. Gao C, Rahaman MN, Gao Q, Teramoto A, Abe K, Robotic deposition and in vitro characterization of 3D gelatin–bioactive glass hybrid scaffolds for biomedical applications. J Biomed Mater Res A 101(7): 2027–37 (2013). doi: 10.1002/jbm.a.34496.
49. Richard RC, Sader MS, Dai J, Thir RMSM, Soares GDA, Beta–type calcium phosphates with and without magnesium: From hydrolysis of brushite powder to robocasting of periodic scaffolds. J Biomed Mater Res A 102A: 3685–3692 (2014). doi: 10.1002/jbm.a.35040
50. Won JE, Mateos–Timoneda MA, Castano O, Planell JA, Seo SJ, Lee EJ, Han CM, Kim HW, Fibronectin immobilization on to robotic–dispensed nanobioactive glass/polycaprolactone scaffolds for bone tissue engineering. Biotechnol Lett 37(4): 935–42 (2015). doi: 10.1007/s10529–014–1745–5.
51. Varanasi VG, Russias J, E, Loomer PM, Tomsia AP. Novel PLA–

and PCL–HA Porous 3D Scaffolds Prepared by Robocasting Facilitate MC3T3–E1 Subclone 4 Cellular Attachment and Growth. In: Biomaterials Science: Processing, Properties, and Applications V: Ceramic Transactions, Volume 254. (2015). https://doi.org/10.1002/9781119190134.ch16.

52. Andrade S, Abdalla A, Montufar E, Corté L, Vanegas P. Fabrication of 3D Bioactive Ceramic Scaffolds by Robocasting. In: Braidot A., Hadad A. (eds) VI Latin American Congress on Biomedical Engineering CLAIB 2014, Paraná, Argentina 29, 30 & 31 October 2014. IFMBE Proceedings, vol 49. Springer, Cham, (2015).

53. MartínezβVázquez F, Pajares A, Miranda P, Effect of the drying process on the compressive strength and cell proliferation of hydroxyapatiteβderived scaffolds. Int J Appl Ceram Technol 14:1101–1106 (2017). https://doi.org/10.1111/ijac.12755.

54. Fiocco L, Elsayed H, Badocco D, Pastore P, Bellucci D, Cannillo V, Detsch R, Boccaccini AR, Bernardo E, Direct ink writing of silica–bonded calcite scaffolds from preceramic polymers and fillers. Biofabric 9: 025012 (2017). https://doi.org/10.1088/1758–5090/aa6c37.

55. Stanciuc AM, Sprecher CM, Adrien J, Roiban LI, Alini M, Gremillard L, Peroglio M, Robocast zirconia–toughened alumina scaffolds: Processing, structural characterisation and interaction with human primary osteoblasts. J Eur Ceram Soc 38: 845–853 (2018). http://dx.doi.org/10.1016/j.jeurceramsoc.2017.08.031.

56. Ben–Arfa BAE, Neto AS, Palamá IE, Salvado IMM, Pullar RC, Ferreira JMF, Robocasting of ceramic glass scaffolds: Sol–gel glass, new horizons. J Eur Ceram Soc 39: 1625–1634 (2019). https://doi.org/10.1016/j.jeurceramsoc.2018.11.019.

57. Liu X, Rahaman MN, Liu Y, Bal BS, Bonewald LF, Enhanced bone regeneration in rat calvarial defects implanted with surface–modified and BMP–loaded bioactive glass (13–93) scaffolds. Acta Biomater 9(7): 7506–7517 (2013). doi: 10.1016/j.actbio.2013.03.039.

58. Deliormanli AM, Liu X, Rahaman MN. Evaluation of borate bioactive glass scaffolds with different pore sizes in a rat subcutaneous implantation model. J Biomater Appl 28(5): 643–653, 2014.

59. Rahaman MN, Lin Y, Xiao W, Liu X, Bal B. Evaluation of Long–Term Bone Regeneration in Rat Calvarial Defects Implanted With Strong Porous Bioactive Glass (13–93) Scaffolds. In book: Biomaterials Science: Processing, Properties, and Applications V. 1, John Wiley & Sons, Ins. New Jersey (2015). DOI: 10.1002/9781119190134.ch9.

60. Lin Y, Xiao W, Liu X, Bal BS, Bonewald LF, Rahaman MN, Long–term bone regeneration, mineralization and angiogenesis in rat calvarial defects implanted with strong porous bioactive glass (13–93) scaffolds. J Non–Cryst Sol 432: 120–129 (2016). http://dx.doi.org/10.1016/j.jnoncrysol.2015.04.008.

61. Simon JL, Michna S, Lewis JA, Rekow ED, Thompson VP, Smay JE, Yampolsky A, Parsons JR, Ricci JL, In vivo bone response to 3D periodic hydroxyapatite scaffolds assembled by direct ink writing. J Biomed Mater Res A, 83(3): 747–58 (2007). https://doi.org/10.1002/jbm.a.31329.

62. Dellinger JG, Eurell JAC, Jamison RD, Bone response to 3D periodic hydroxyapatite scaffolds with and without tailored microporosity to deliver bone morphogenetic protein 2. J Biomed Mater Res A 76(2): 366–76 (2006). DOI: 10.1002/jbm.a.30523.

63. Luo Y, Zhai D, Huan Z, Zhu H, Xia L, Chang J, Wu C. Three–Dimensional Printing of Hollow–Struts–Packed Bioceramic Scaffolds for Bone Regeneration. ACS Appl. Mater. Interfaces 7: 24377–24383 (2015). doi: 10.1021/acsami.5b08911.

64. Lin KF, He S, Song Y, Wang CM, Gao Y, Li JQ, Tang P, Wang Z, Bi L, Pei GX, Low–Temperature Additive Manufacturing of Biomimic Three–Dimensional Hydroxyapatite/Collagen Scaffolds for Bone Regeneration. ACS Appl Mater Interfaces 8(11): 6905–6916 (2016). https://doi.org/10.1021/acsami.6b00815.

65. Shao H, Liu A, Ke X, Sun M, HE Y, Yang X, Fu J, Zhang L, Yang G, Liu Y, Xu S, Gou Z, 3D Robocasting Magnesium–doped Wollastonite/TCP Bioceramics Scaffolds with Improved Bone Regeneration Capacity in Critical Sized Calvarial Defects. J Mater Chem B 5(16): 2941–2951 (2017). doi: 10.1039/C7TB00217C.

66. Zheng J, Carlson WB, Reed JS, Dependence of compaction efficiency in dry pressing on the particle size distribution. J Am Ceram Soc 78(9): 2527–2533 (1995).

67. Konakawa Y, Ishizaki K, The particle size distribution for the highest relative density in a compacted body. Powder Technol 63: 241–246 (1990).

68. Zheng J, Carlson WB, Reed JS, The packing density of binary powder mixtures. J Eur Ceram Soc 15: 479–483 (1995).

69. Ferreira JMF, Diz HMM, Effect of the amount of deflocculant and powder size distribution on the green properties of silicon carbide bodies obtained by slip casting. J Hard Mater 3: 17–27 (1992).

70. Taruta S, Takusagawa N, Okada K, Otsuka N, Slip casting of alumina powder mixtures with bimodal size distribution. J Ceram Soc Japan 104: 47–50 (1996).

71. William JH, Zukoski CF, The rheology of bimodal mixtures of colloidal particles with long–range, soft repulsions. J Colloid Interface Sci 210: 343–351 (1999).

72. Olhero S, Ferreira JM, Influence of particle size distribution on rheology and particle packing of silica–based suspensions. Powder Technol 139(1): 69–75 (2004). doi:10.1016/j.powtec.2003.10.004

73. Nutz M, Furdin G, Medjahdi G, Marêché GF, Moreau M, Rheological properties of coal tar pitches containing micronic graphite powders. Carbon 35: 1023–1029 (1997).

74. Yuan J, Murray HH, The importance of crystal morphology on the viscosity of concentrated suspensions of kaolins. Appl Clay Sci 12: 209–219 (1997).

75. Joseph R, McGregor WJ, Martyn MT, Tanner KE, Coates PD, Effect of hydroxyapatite morphology/surface area on the rheology and processability of hydroxyapatite filled polyethylene composites. Biomater 23(21): 4295–4302 (2002). doi:10.1016/s0142–9612(02)00192–8

76. Feilden E, Ferraro C, Zhang Q, García–Tuñón E, D'Elia E, Giuliani F, Vandeperre L, Saiz E. 3D Printing Bioinspired Ceramic Composites. Sci Rep 7: 13759 (2017). https://doi.org/10.1038/s41598–017–14236–9

77. Miranda P, Saiz E, Gryn K, Tomsia AP, Sintering and robocasting of β–tricalcium phosphate scaffolds for orthopaedic applications. Acta Biomater 2(4): 457–466 (2006). doi:10.1016/j.actbio.2006.02.004

78. Eqtesadi S, Motealleh A, Miranda P, Pajares A, Lemos A, Ferreira, JMF, Robocasting of 45S5 bioactive glass scaffolds for bone tissue engineering. J Eur Ceram Soc 34(1): 107–118 (2014). doi:10.1016/j.jeurceramsoc.2013.08.003

79. Zhang D, Peng E, Borayek R, Ding J. Controllable Ceramic Green–Body Configuration for Complex Ceramic Architectures with Fine Features. Adv Funct Mater 1807082 (2019). doi:10.1002/adfm.201807082

80. He G, Hirschfeld DA, Cesarano J (n.d.), Processing and Mechanical Properties of Silicon Nitride Formed by Robocasting Aqueous Slurries, in Ceramic Engineering and Science Proceedings, 607–614 (2000). doi:10.1002/9780470294635.ch72

81. Glymond D, Vandeperre LJ, Robocasting of MgO–doped alumina using alginic acid slurries. J Am Ceram Soc 101(8): 3309–3316 (2018). doi:10.1111/jace.15509

82. Schlordt T, Schwanke S, Keppner F, Fey T, Travitzky N, Greil P, Robocasting of alumina hollow filament lattice structures. J Eur Ceram Soc 33(15–16): 3243–3248 (2013). doi:10.1016/j.jeurceramsoc.2013.06.001

83. Powell J, Assabumrungrat S, Blackburn S, Design of ceramic paste formulations for co–extrusion, Powder Technol 245:21–27 (2013).

84. Bourret J, El Younsi I, Bienia M, Smith A, Geffroy PM, Marie J, Ono Y, Chartier T, Pateloup V, Micro extrusion of innovative alumina pastes based on aqueous solvent and eco–friendly binder. J Eur Ceram Soc 38(7): 2802–2807 (2018).

85. Faes M, Valkenaers H, Vogeler F, Vleugels J, Ferraris E, Extrusion–based 3D Printing of Ceramic Components, in Procedia CIRP 28: 76–81 (2015).

86. Li W, Ghazanfari A, McMillen D, Leu MC, Hilmas GE, Watts J, Characterization of zirconia specimens fabricated by ceramic on–demand extrusion. Ceram Int 44(11): 12245–12252 (2018).

87. Azzolini A, Sglavo VM, Downs JÁ, Novel method for the identification of the maximum solid loading suitable for optimal extrusion of ceramic pastes. J Adv Ceram 3(1): 7–16 (2014).

88. Franks GV, Tallon C, Studart AR, Sesso ML, Leo S, Colloidal processing: enabling complex shaped ceramics with unique multiscale structures. J Am Ceram Soc 100(2): 458–490 (2017). doi:10.1111/jace.14705

89. Ben–Arfa BAE, Neto AS, Miranda Salvad IM, Pullar RC, Ferreira JMF, Robocasting: Prediction of ink printability in solgel bioactive glass. J Am Ceram Soc 102(4): 1608–1218 (2018). doi:10.1111/jace.16092

90. Stickel JJ, Powell RL, Fluid mechanics and rheology of dense suspensions. Annu Rev Fluid Mech 37: 129–149 (2005). doi: 10.1146/annurev.fluid.36.050802.122132

91. Schlordtil T, Greil P, Robocasting of Alumina Lattice Truss Structures. J Ceram Sci Technol 3(2): 81–8 (2012).

92. Smay JE, Cesarano J, Lewis JA, Colloidal Inks for Directed Assembly of 3–D Periodic Structures. Langmuir, 18(14), 5429–5437 (2002). doi:10.1021/la0257135

93. Lewis JA, Colloidal Processing of Ceramics. J Am Ceram Soc 83(10): 2341–2359 (2004). doi:10.1111/j.1151–2916.2000.tb01560.x

94. Wahl L, Lorenz M, Biggemann J, Travitzky N, Robocasting of reaction bonded silicon carbide structures, J Eur Ceram Soc 39(15): 4520–4526 (2019).

95. M'Barki A, Bocquet L, Stevenson A, Linking Rheology and Printability for Dense and Strong Ceramics by Direct Ink Writing. Scientific Reports 7:6017 (2017).

96. Wolfs, R.J.M., Suiker, A.S.J. Structural failure during extrusion–based 3D printing processes. Int J Adv Manuf Technol 104, 565–584 (2019). https://doi.org/10.1007/s00170–019–03844–6franks

97. Lui YS, Sow WT, Tan LP, Wu Y, Lai Y, Li H, 4D Printing and Stimuli–responsive Materials in Biomedical Applications. Acta Biomater 92: 19–36 (2019).

98. Gao B, Yang Q, Zhao X, Jin G, Ma Y, Xu F, 4D Bioprinting for Biomedical Applications. Trends Biotechnol 34(9): 746–756 (2016).

99. Liu G, Zhao Y, Wu G, Lu J, Origami and 4D printing of elastomer–derived ceramic structures. Sci Adv 4: eaat0641 (2018).

100. Tamay DG, Dursun Usal T, Alagoz AS, Yucel D, Hasirci N and Hasirci V, 3D and 4D Printing of Polymers for Tissue Engineering Applications. Front Bioeng Biotechnol 7:164 (2019). doi: 10.3389/fbioe.2019.00164

101. Bargardi, F., Le Ferrand, H., Libanori, R. et al. Bio–inspired self–shaping ceramics. Nat Commun 7: 13912 (2016). https://doi.org/10.1038/ncomms13912

102. Franchina G, Scanferla P, Zeffiro L, Elsayed H, Baliello A, Giacomello G, Pasetto M, Colombo P, Direct ink writing of geopolymeric inks. J Eur Ceram Soc 37: 2481–2489 (2017).